ELSEVIER

Journal of Chromatography A, 883 (2000) 11–25

JOURNAL OF CHROMATOGRAPHY A

www.elsevier.com/locate/chroma

Hydrodynamic aspects of slurry packing processes in microcolumn liquid chromatography

Johannes P.C. Vissers[a,*], Martijn A. Hoeben[b], Jozua Laven[b], Henk A. Claessens[a], Carel A. Cramers[a]

[a]*Laboratory of Instrumental Analysis, Eindhoven University of Technology, P.O. Box 513, 5600 MB, Eindhoven, The Netherlands*
[b]*Laboratory of Polymer Chemistry and Coatings Technology, Eindhoven University of Technology, P.O. Box 513, 5600 MB Eindhoven, The Netherlands*

Received 17 December 1999; received in revised form 15 February 2000; accepted 21 February 2000

Abstract

A Stokesian dynamics computer simulation based method is presented for the estimation of the bed porosity of slurry-packed capillary liquid chromatography (LC) columns. A colloidally well-described reversed-phase stationary phase–slurry liquid suspension was used as a model system. The applied simulation method takes into account the velocity of the slurry and colloidal interaction forces, as well as inter-particle hydrodynamic interactions. The predicted bed porosities suggest that a lower slurry velocity leads to a denser packing structure due to the increased effect of colloidal repulsion effects. The results of the simulations were compared with the external porosity and chromatographic performance of capillary LC columns that were packed at different filtration and compaction pressures. However, the trends that were observed in the experimental results suggest that hydrodynamic packing parameters have no or little effect on the chromatographic performance of capillary LC columns. Within the experimental parameter window, the chromatographic performance and the column porosity were not influenced by the filtration and compaction pressure, nor by the duration of the compaction process.

Keywords: Slurry packing; Computer simulation; Bed porosity; Stationary phases, LC

1. Introduction

The packing of microcolumns is–according to Verzele–a matter of technique [1]. In line with this view, many different packing techniques have been suggested to efficiently fill microcolumns. The most commonly applied packing techniques the use of stationary phase slurries for the transport of the particles to the capillary column. Early studies on this technique [2–8] primarily examined the effect of the selection of the slurry solvent. Other ways to transport stationary phase particle into a capillary LC column are the use of gases [9–11] or supercritical fluids [12–17]. The majority of these techniques have in common that they are based on trial-and-error methods and assumptions. Despite this, all these methods seem to provide more or less equal, acceptable column performance with reduced plate heights only slightly higher or equal to 2 for columns with an internal diameter (I.D.) of 150 to 500 μm.

*Corresponding author. Present address: LC Packings, Baarsjesweg 154, 1057 HM Amsterdam, The Netherlands. Tel.: +31-20-683-9768; fax: +31-20-685-3452.

0021-9673/00/$ – see front matter
PII: S0021-9673(00)00276-4

Several studies have been published that report on the preparation of microcolumns in more detail. The coagulating properties of stationary phase materials in slurry and packing liquids–and their effect on the chromatographic performance–was studied by Shelly and Edkins [18] and Vissers et al. [19,20]. The two latter papers demonstrated a particle-settling–velocity based method to quantitatively describe the extent of particle coagulation, whereas the former one was more qualitatively based. The studies of both research groups indicated that the use of a packing liquid in which the stationary phase particles coagulated was favorable. Other papers focussed more on the effect of the packing pressure and packing velocity. One of the first papers that described the effect of the packing time on the performance of capillary LC column was published by Gluckman et al. [21]. At about the same time Meyer and Hartwick [22] presented a systematic evaluation on the packing of 1.0 mm I.D. columns with irregularly shaped particles at constant velocity or constant pressure. Also Shelly et al. [23] reported on the performance of microcolumns packed at constant velocity and constant pressure. However, their study involved the packing of capillary sized columns of 250 μm I.D. with spherical particles. Others have reported on the effect of the packing pressure on the LC column properties as well, but those studies involved conventional, large I.D. high-performance liquid chromatography columns [24,25]. Zimina and coworkers [26,27] related the kinematic viscosity of the slurry liquid and the column performance of 500 μm I.D. packed polyetheretherketone columns. It was shown that detergent-containing slurry liquids lowered the kinematic viscosity of the slurry suspension, which had a favorable effect on the column performance. A lower slurry viscosity increases however the packing velocity, but this was not included in their studies.

The slurry-packing process of an LC column can be divided into five consecutive steps: (1) stationary phase–slurry preparation, (2) transfer of the stationary phase–slurry to the slurry vessel, (3) filtration of the stationary phase–slurry through the column to form the particle bed, (4) compaction of the obtained stationary phase particle bed and (5) conditioning of the stationary phase particle bed. This work deals with steps (3) and (4) and is part of a systematic study on the influence of each of these five individual steps on the final column properties. Previously, work was published on steps (1) and (2), where the effect of particle coagulation in packing and slurry liquids was investigated and related to the performance of capillary LC columns [19,20]. However, in these previous studies the effect of the particle filtration rate–i.e. step (3) in the column packing process–was not examined. This paper deals explicitly with the theoretical and practical aspects of the particle filtration speed in column slurry-packing processes. The bed porosity and chromatographic performance of simulated bed structures were predicted by means of a Stokesian-dynamics computation method. The investigated parameters included filtration velocity and filtration pressure. The applied calculation method also took into account colloidal attraction and repulsion forces. The results of the simulation experiments were compared with practically obtained chromatographic results from a series of experiments where both the filtration and packing pressure was varied. In addition, the columns were characterized with respect to their bed porosity. Explanations for the discrepancies between theory and practice are suggested.

2. Theory

The dynamics of the particles are determined by several forces associated with colloidal interaction, hydrodynamics and Brownian motion. Generally speaking, dealing with the ‘multi’-particle hydrodynamic interactions remains the most difficult part in the mathematical description of suspension flow simulations. The complex nature of the hydrodynamic interactions arises from the fact that part of the actual hydrodynamic forces experienced by particles are the result of a local fluid velocity fields that induce infinite series of interparticle interactions. This can be seen as follows: the movement of a sphere implies the movement of the fluid around it. Other spheres that are in the vicinity will experience the velocity field induced by the first sphere and will respond by moving. The movements of the other

spheres affect the velocity field too, which again influences the movement of the first sphere. The motion of the spheres and the fluid are thus an infinite cascade of responses. Whatever the complexity of the individual forces on the particles may be, the force balance for an individual particle is expressed by the Langevin-equation:

$$m\frac{dv}{dt} = F_H + F_B + F_P \quad (1)$$

where m is the mass of the sphere, F_H is the hydrodynamic force, F_B the Brownian force and F_P the colloidal interaction force plus the gravity. If the accelerations of the particles are sufficiently small, the term mdv/dt can be neglected. Hence, a pseudo-equilibrium situation exists–i.e. at every moment the sum of forces on each particle equals zero. In case the Brownian force F_B can be neglected as well–which is realistic in case the particle diameter is typically 5 μm or more–Eq. (1) reduces to:

$$F_H = -F_P \quad (2)$$

which states that at any moment in time the total hydrodynamic drag on a particle is the opposite of all the colloidal interaction forces. F_P is composed of two types of interactions with neighboring particles: Van der Waals attraction and electrostatic repulsion [28]. The force F_P on a spherical particle j, with radius a, constant surface potential Ψ_0 and Hamaker constant A_{12} is equal to:

$$F_{DLVO,j} = \sum_{i \neq j} -\frac{A_{12}a}{12h_{ij}^2} + 2\pi\varepsilon_r\varepsilon_0 a\Psi_0^2 \frac{e^{-\kappa h_{ij}}}{1+e^{-\kappa h_{ij}}} \quad (3)$$

where h_{ij} is the distance between the surfaces of particles i and j, ε_r is the relative dielectric constant of the fluid, ε_0 is the permittivity of vacuum and κ^{-1} the double layer thickness. The summation has to be performed over all particles in the suspension apart from particle j itself. With Eq. (3), F_P can be calculated and subsequently from Eq. (2), the hydrodynamic force F_H on each particle. Using hydrodynamics, the velocities v of the particles can be calculated once the forces on the particles are known. This allows to estimate the displacements $\Delta x = v \cdot \Delta t$ after a short time interval Δt. In this way, a new configuration of the suspension can be calculated and the process–starting with the calculation of F_P can be repeated. As mentioned before, the most difficult step in this procedure is the calculation of the velocities from F_H.

In this section it will be explained briefly how this problem is solved in the Stokesian dynamics method. Stokesian dynamics is a simulation method which can be used to model the dynamics when inertia forces are negligible, as is usually the case with suspensions. In that case, flow in the liquid phase is governed by the Stokes equation:

$$\nabla \cdot v = 0 \quad (4)$$

and the equation of continuity:

$$-\nabla p + \eta\nabla^2 v + f = 0 \quad (5)$$

where ∇ is the differential vector operator, p is the hydrodynamic pressure, η is the fluid viscosity, v is the particle velocity and f is the force per unit volume. These 'creeping' flow equations are basically a simplified form of the Navier–Stokes equations and are only valid in case the flow around the particles in the suspension is laminar, i.e. Re«1, where $Re = 2\rho\Delta v a/\eta$ where ρ is the fluid density and Δv is the velocity difference between the fluid and the particle. Re«1 is usually valid for colloidal systems because a is small. Solving the set of Eqs. (4) and (5) together with the boundary conditions for a given system–e.g. the definition of the fluid velocity at the borders of the fluid–results in functions describing the fluid velocity field v and dynamic pressure field p as a function of the position x.

An important feature of the creeping flow equations is the fact that they are both linear differential equations. This means that the relation between the velocities v and annular velocities Ω of the spheres on the one hand and the forces F and torques T applied to them on the other hand is a linear relation as well. Mathematically this can be expressed as:

$$\begin{bmatrix} v_{1,x} \\ v_{1,y} \\ v_{1,z} \\ \Omega_{1,x} \\ \Omega_{1,y} \\ \Omega_{1,z} \\ v_{2,x} \\ \cdot \\ \cdot \\ \cdot \\ \cdot \\ \cdot \\ \cdot \\ \Omega_{N,y} \\ \Omega_{N,z} \end{bmatrix} = \begin{bmatrix} \mu_{11} & \mu_{12} & \mu_{13} & \cdot & \cdot & \cdot & \mu_{16(N)} \\ \cdot & & & & & & \cdot \\ \cdot & & & & & & \cdot \\ \cdot & & & & & & \cdot \\ \cdot & & & & & & \cdot \\ \cdot & & & & & & \cdot \\ \cdot & & & & & & \cdot \\ \cdot & & & & & & \cdot \\ \cdot & & & & & & \cdot \\ \cdot & & & & & & \cdot \\ \cdot & & & & & & \cdot \\ \cdot & & & & & & \cdot \\ \cdot & & & & & & \cdot \\ \mu_{6(N)1} & & & & & & \mu_{6(N)6(N)} \end{bmatrix} \begin{bmatrix} F_{1,x} \\ F_{1,y} \\ F_{1,z} \\ T_{2,x} \\ T_{2,y} \\ T_{2,z} \\ F_{2,x} \\ \cdot \\ \cdot \\ \cdot \\ \cdot \\ \cdot \\ \cdot \\ T_{N,y} \\ T_{N,z} \end{bmatrix} \quad (6)$$

where μ is the $6N \times 6N$-dimensional mobility matrix that can be derived from the underlying quasi full-body multi-particle hydrodynamics theory. V_{ij} and F_{ij} are the velocity and force of particle i in the j-direction. Ω_{ij} is the rotational speed of particle i around the j-axis. Relation (6) is referred to as the mobility equation. An efficient method to calculate the elements of μ was first proposed by Durlofsky et al. [29]. Their approach is based on describing local fluid velocities as linear functions of the forces, torques and so-called higher order multipole moments of the forces by means of Taylor expansions. These higher order multipoles are related to the force distribution on the particles.

In order to avoid unpractically long computation times, the number of multipoles included in the calculation is restricted. However, in order to account for an adequate calculation of short-range interactions when two individual particles almost touch each other, a substantial number of multipoles have to be included. Durlofsky et al. dealt with this problem in an approximated, yet accurate way. They understood that this part of the higher multipoles of the multi-particle interactions can be adequately approximated with the much simpler result for two-particle interaction. Thus, they added the exact, known two-body mobility matrices to the many-particle mobility matrix μ, the latter containing only a limited number of multipoles. In contrast to μ, these two-particle mobility matrices do not show a many-particle character. Simulations performed for clusters consisting of five to fifteen particles showed that the precision is acceptable even when many-particle multipoles of only the zeroth and first order are included in the calculation.

Recently, Hinsen and coworkers [30] have developed a computer program called 'Hydrolib', which allows the efficient calculation of many-body mobility matrices for spheres in creeping flow. The method used is outlined by Chichocki et al. [31] and is in fact in many aspects analogous to the method proposed by Durlofsky et al. An important difference is however that Hydrolib is capable of performing relatively fast calculations when a higher number of multipole moments are to be included. It was argued by Chichocki et al. that for clusters larger than about ten spheres, truncation after the first multipole moment is unacceptable.

3. Experimental section

3.1. Simulation experiments

All calculations were performed on a Silicon Graphics Power Challenge XL super computer (Mountain View, CA) for BioSil C_{18} HL 90-5 S in acetone–which will also be one of the stationary phase–solvent system studied in the chromatographic section of this paper. The relevant physical constants for this system are listed in Table 1. The perception of such a set of parameters is described in a previous paper, where the physical constants of other stationary phase–solvent systems can be found too [20].

3.2. Column construction and packing equipment

Columns were constructed from 40 cm×320-μm

Table 1
Physical constants for the system BioSil C_{18} HL 90-5 S-acetone

Physical constant	Symbol	Value
Hamaker attraction constant	A	$8.8 \cdot 10^{-21}$ J
Surface potential	ψ_0	$-84.5 \cdot 10^{-3}$ V
Double layer thickness	κ^{-1}	$3.13 \cdot 10^{-7}$ m^{-1}
Particle radius	a	$2.65 \cdot 10^{-6}$ m
Di-electric constant	ε_r	21.0
Solvent viscosity	η	$0.32 \cdot 10^{-3}$ Pa s
Solvent density	ρ	$0.79 \cdot 10^{3}$ kg m^{-3}
Particle radius (used in simulations)	a	$2.50 \cdot 10^{-6}$ m

I.D. uncoated fused-silica tubing (Chrompack, Middelburg, The Netherlands). An EPM2000 glass filter frit (Whatman, Maidstone, UK) was cut out by the column. To hold the frit in position an 8 cm×75-μm I.D./280-μm outer diameter (O.D.) fused-silica capillary (Polymicron Technologies, Phoenix, AZ) was fixed into the larger capillary using a two-component epoxy resin.

The packing equipment consisted of a DSTV-122 air driven fluid pump (Haskel Eng., Burbank, CA) for constant pressure packing and a 19 cm×2 mm I.D. stainless-steel slurry reservoir. The column was connected to the slurry vessel by means of a home made double cone. Stationary phase slurries were prepared at a concentration of 100 mg ml^{-1} in acetone by sonication for 10 min. Afterwards, the slurry was transferred to the slurry reservoir with a syringe and pneumatically pumped in the capillary. This typically took less then 2 min. Thereafter, the packing pressure was maintained for 30 min unless stated otherwise.

3.3. Magnetic resonance imaging

Magnetic Resonance Imaging (MRI) experiments were conducted at room temperature on a 0.47 T imager consisting of a Bruker electromagnet (Rheinstetten/FO., Karlsruhe, Germany), a SMIS console and a DOTY probe head with actively shielded gradients and a 4.5 cm diameter cylindrical sample space. The capillary LC columns were placed together with a test tube that contained neat, stagnant mobile phase doped with a small amount of $MnCI_2$ for reference measurements in the sample space. Magnetic field gradients were applied by means of a home-made transmitter/receiver coil with a diameter of 1 cm and a length of 3 cm. The spatial resolution of the applied MRI equipment was 80×80×3000 μm in the *x*, *y* and *z*-direction respectively, where the *z*-direction was directed along the column axis. Hence, at each axial position *z* a maximum of about 12 displacement profiles could be probed in each 300 μm I.D. capillary–in practice about eight profiles could be analyzed. Details on the MRI equipment and the applied pulse sequences are published by the group of Van As [32,33].

In this study, three capillary LC columns were subjected to MRI measurements to study the feasibility of this technique to study the local porosity of the chromatographic bed in capillary LC columns. To this extent, two columns that were packed at different filtration pressures were studied and a reference column that was expected to have a distinctly different bed structure. The latter column had in fact a very poor chromatographic performance-reduced plate height $h \approx 32$–and a column resistance factor that is about two to three times as high as normally would be expected. The packing conditions for preparing such an exceptionally performing column can be found elsewhere [19]. Each column was measured at five different axial positions–i.e. at a distance in between 10 to 15 cm from the column outlet frit–over the whole capillary length.

3.4. Chromatographic instrumentation

The capillary LC system consisted of a model 100 DM syringe pump (ISCO Inc., Lincoln, NE), a 785A Programmable Absorbance detector (Applied Biosystems, San Jose, CA) equipped with a capillary flow cell (LC Packings, Amsterdam, The Netherlands), and a 200 nl CI4W injection valve (VICI-AG Valco Europe, Schenkon, Switzerland). A 0.2-μm nylon membrane (Alltech Associates Inc., Deerfield, IL) was positioned into the valve outlet to the column to circumvent stationary phase particles entering the injection valve. UV detection was performed at 254 nm. A 900 Series Interface and Nelson 5.0 software (Perkin-Elmer Nelson, Cupertine, CA) were used for data acquisition.

3.5. Column evaluation

The reversed-phase capillary LC columns were evaluated with a test-mixture containing four components: uracil (dead volume marker), naphthalene, phenanthrene and anthracene. The concentration of all components was approximately $1 \cdot 10^{-4}$ mol l^{-1}. An acetonitrile/water (70:30, v/v) mixture was used as the mobile phase. The individual solvents of the mobile phase were filtered through a 0.45-μm filter. Prior to use, the mobile phase was degassed with helium. The peak of anthracene was used to calculate the column efficiencies. Plate heights were calculated using an algorithm developed by Foley and Dorsey

[34]. In addition, extra column bandbroadening effects were accounted for.

3.6. Chemicals

Acetone was purchased from Merck (Darmstadt, Germany). Uracil, anthracene, naphthalene and phenanthrene were from Fluka AG (Buchs, Switzerland). All chemicals were of p.a. grade. Water was purified and demineralized with a Milli-Q water purification system (Waters–Millipore Milford, MA) prior to use. The reversed-phase stationary phase BioSil C_{18} HL 90-5 5 was from BioRad RSL nv. (Nazareth, Belgium).

4. Results and discussion

4.1. Simulation of one particle while being filtrated on a packed bed

In practice, packing of a bed is carried out with a fairly concentrated slurry-volume fraction $\phi = 0.10$. When the particles approach the bed, they will interact with each other and with the bed. The interaction of individual particles with the bed may prevail close to the bed. Thus the approach of a single particle towards the bed was investigated as it is expected to give qualitative insight in phenomena like coagulation and whether the packing is ballistic rather than colloidal in nature.

A photographic representation of this experiment is given in Fig. 1. A virtual bed was composed of 72 immobile particles organized in two layers. The particles in the top layer are above the holes in the lower layer. In fact, the bed consisted of two infinite layers, in view of the imposed periodic boundary conditions. The inter-particle distances are given in Fig. 1. The freely moving particle was positioned right above one of the particles in the upper layer of the bed. A liquid flow was imposed normal to the bed, which forced the particle to move towards the bed. If the distance between the surface of the freely moving particle and the surface of the closest particle in the bed is fairly great, the particle's velocity is hardly influenced by the presence of the bed and it will move with the fluid velocity v_∞. At close range however, its velocity will change appreciable due to hydrodynamic and colloidal interaction forces. At a surface-to-surface distance $h_{ij} = a$ the effect amounts to a velocity alteration of approximately 4%. At this range of distances the colloidal interaction forces are still very small and the effect is entirely hydrodynamic. How hydrodynamics change the particle speed v_0 in the absence of colloidal interactions is shown in Fig. 2. As the particle approaches further, the hydrodynamic resistance will steadily grow and eventually become so high that a true collision between the freely moving particle and the one in the bed cannot occur in the absence of some attractive force. The dashed line reflects the theoretical slope of the curve. At such small distances, however, the

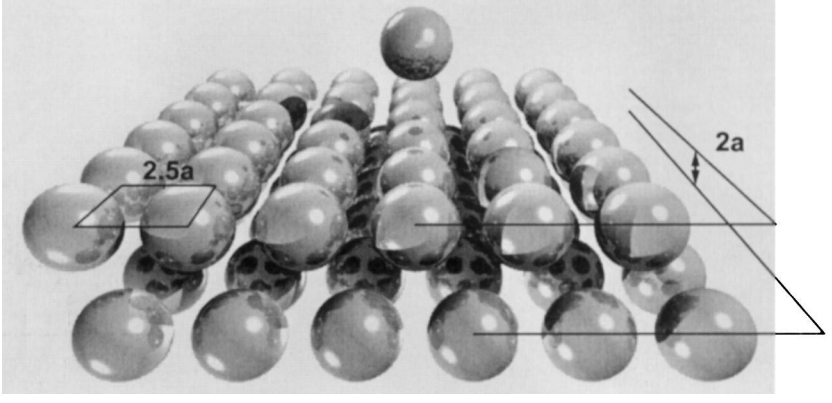

Fig. 1. Photographic representation of the effect of colloidal interaction forces on the movement of a single particle approaching a bed. The freely moving particle is positioned exactly above one of the particles of the top layer of an entirely flat bed.

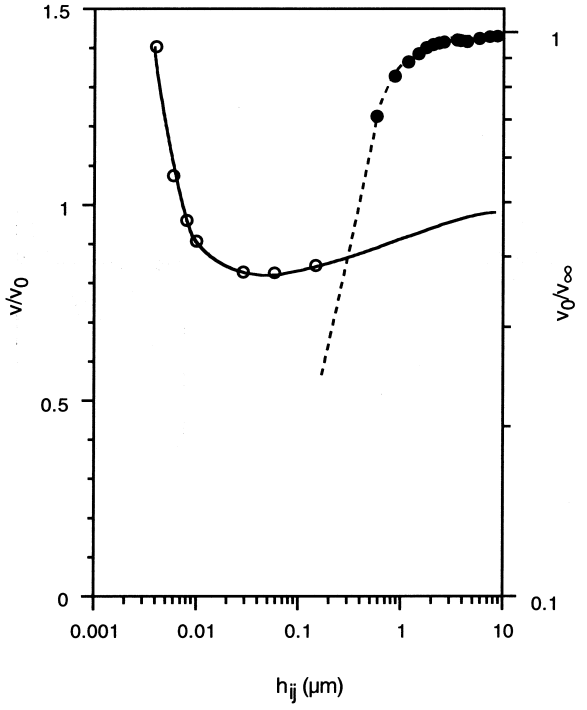

Fig. 2. The relative change in velocity of a freely moving particle as a function of the particle-to-particle distance h_{ij} for the hypothetical situation considered in Fig. 1. The hydrodynamic effect in the absence of colloidal forces v_0/v_∞ and the influence of colloidal forces v/v_0. See the text for details.

colloidal repulsive and attractive forces become significant. The effect of these colloidal interaction forces is also shown in Fig. 2. The velocity of a dragged particle was calculated in case colloidal interaction forcus were present v and absent v_0. The ratio of these two velocities is plotted versus the distance h_{ij} between the surface of the freely moving particle and the surface of the particle of the bed being approached.

It can be seen that $v/v_0<1$ for $h_{ij}>7$ nm, which means that the colloidal interaction forces will slow down the particle even more, due to electrostatic repulsion. If h_{ij} becomes less than 7 nm, the attractive Van der Waals force starts to dominate which leads to almost instantaneous coagulation. Furthermore, it can be seen that in the region beyond 7 nm, the effect of the presence of the DLVO force on the particle velocity is always modest. This means that the retardation of the particles is mainly determined by hydrodynamic forces between the particle and the virtual bed.

4.2. Simulation of the evolution of a packed bed structure

This section discusses the results of simulations of the filtration of a stationary phase suspension at different fluid velocities. A set of 600 particles randomly placed in a cubic unit cell was used as the start configuration for all simulations. The foot print of the unit cell was taken as 15 times the particle radius a in both the x and y-direction. The height of the unit cell equalled 112 times a implying a slurry particle volume fraction of 0.1. A virtual frit–composed of four layers of 36 fixed particles–was placed at the bottom of the unit cell. The distances between the virtual frit particles was the same as those in Fig. 1. A representation of the starting conditions is given in Fig. 3.

Only those moving particles that were in the proximity of the stationary bed were taken into account in the mobility calculation. To this extent a cubic cell with edges of $15a$ was defined. A particle with its centre in the top plane of this cube is at a distance of $4a$ to the stationary bed. The total number of particles in this box was kept constant for numerical reasons. This implies however that an appropriate number of particles at the bottom of the box had to be removed during the simulations, particles that were not included in the mobility calculation were moving with the fluid velocity. Throughout the simulations it was checked if the mobility calculation included particles that formed a bed of at least one layer thick.

Colloidal interactions between particles up to a distance of $15a$–including periodic images–were taken into account. The time step size was set to $2.7\cdot10^{-7}$ m v_{fluid}^{-1}. If the particle-to-bed distance was smaller than 0.7 nm the particles were considered to be coagulated. In case of particle overlap–a numerical problem related to the size of the time step–the interparticle distance was set at 0.7 nm. The existence of aggregates in the slurry was not taken into account since (i) the suspension is colloidally stable and (ii) the near absence of shear flow–implying very few collisions in the suspension. The possibility of rolling after coagulation was not included in the

Fig. 3. Start configuration for the simulations of the packing process. The virtual frit consisted of 144 particles which are ordered in four equidistant layers at a distance of two times the particle radius a of each other. The total number of spheres was equal to 600. The unit cell has a length of $15a$ in the x and y-direction and $122a$ in the z-direction.

simulations. In total three of such simulations were conducted. Although rolling would possibly have led to somewhat higher densities, it will not modify the trend of the effect of velocity on the bed density, because viscosity-induced rolling is basically a hydrodynamic problem and scales with the product of viscosity and time. In the first two simulations the total number of particles included in the mobility calculation equalled 98 and in the third one the total number of particles was 150. The fluid velocities were respectively $0.3\cdot10^{-3}$, $5\cdot10^{-3}$ and $11.5\cdot10^{-3}$ $\mathrm{m\,s^{-1}}$. As a reference, also the purely ballistic situation was investigated, i.e. the settlement of particles in a straight line. A representation of the obtained bed structures is given in Fig. 4.

The simulated bed structures were characterized based on their external porosity ε_u, which is defined as:

$$\varepsilon_u = \frac{V_{void}}{V_{voids} + V_{particles}} \tag{7}$$

where V_{void} is the inter-particle volume and $V_{particles}$ is the total volume occupied by the particles. A limitation of this characterization method is however that no information k, is obtained about the presence of irregularities in the simulated bed. The dimension and the total volume of the voids was accessed by positioning randomly a number of mathematical points in the bed structure. The number of points placed within particles reflects the volume fraction of particles within the simulated bed structure. For the points placed outside the particles, the radius of the largest sphere was determined that could be centered at these points without touching a particle in the formed bed. The number of hits as a function of the radius of the largest fitting sphere–i.e. the area under the resulting curves–provides information about ε_u. All curves were computed by randomly scanning 36 000 points in a volume of $15a\times15a\times20a$. The external porosity ε_u was found to be 0.55 for fluid velocities of $11.5\cdot10^{-3}$ and $5\cdot10^{-3}$ $\mathrm{m\,s^{-1}}$. For a fluid velocity of $0.3\cdot10^{-3}$ $\mathrm{m\,s^{-1}}$, ε_u was 0.45. For the purely ballistic situation ε_u was found to be equal to 0.76.

A more illustrative method for assessing the anisotropy of the pores is by both placing horizontally and vertically orientated lines–i.e. x and z-direc-

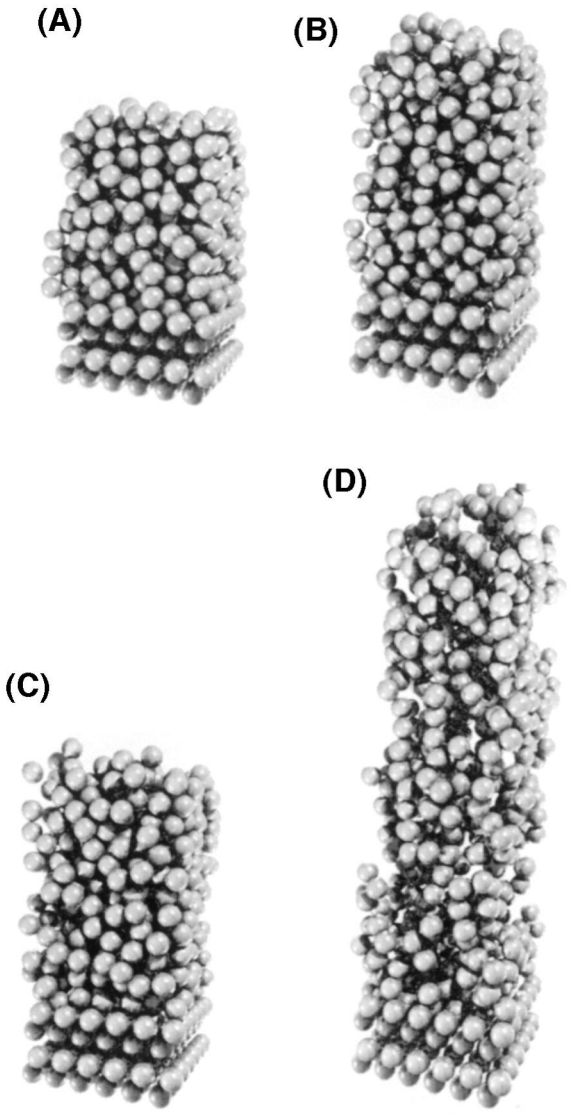

Fig. 4. Photographic representation of the bed structures obtained after simulation with a fluid velocity of $0.3\cdot10^{-3}$ m s^{-1} (A), $5\cdot10^{-3}$ m s^{-1} (B) and $11.5\cdot10^{-3}$ m s^{-1} (C). Structure (D) represents the particle bed in case of a purely ballistic situation, i.e. settlement of the particles in a straight line.

tion respectively–through points randomly positioned outside the particles. The lines were given lengths so as they just touched the particles. The lengths of the horizontally and vertically placed lines–h_x and h_z respectively–provide information about the volume and the shape of the voids. The results of this method are shown in Fig. 5 for the three bed structures that were obtained by simulation and for the ballistic simulated bed structure. The number of points that was scanned in this way was 288 000 in a volume of $15a\times15a\times20a$.

The differences between the porosity values and the void sizes obtained at $11.5\cdot10^{-3}$ and $5\cdot10^{-3}$ m s^{-1} on one hand and at $0.3\cdot10^{-3}$ m s^{-1} at the other hand is remarkable. The bed structure obtained at the lowest fluid velocity is much denser then that at the two higher velocities, implying that the effect of colloidal interaction forces is significantly larger at a fluid velocity of $0.3\cdot10^{-3}$ m s^{-1} than at $5\cdot10^{-3}$ and $11.5\cdot10^{-3}$ m s^{-1}. Higher colloidal repulsion forces lead to a denser bed. The approaching particle is held away from the bed surface so it can move sideway to find a better lower fit. The fact that the bed porosities and the void sizes are comparable at fluid velocities of $5\cdot10^{-3}$ and $11.5\cdot10^{-3}$ m s^{-1} suggests that the filtration process at these fluid velocities is completely determined by hydrodynamic forces and colloidal forces are negligible. Based on the results shown in Fig. 5 it is concluded that in all cases expect the ballistic one, the majority of the voids is smaller than the particle radius of 2.5 μm. Only in the case of ballistic filtration a considerable part of the voids have dimensions larger than the particle diameter.

4.3. Application of the simulation experiments to practical filling conditions

In the simulations a flat fluid velocity profile was assumed. However, in practice a parabolic fluid profile $v_z(r)$ will exist within the capillary. Its effect is most pronounced near the wall. The parabolic fluid profile is described by Poiseuille's law:

$$v_z(r) = \frac{\Delta p d_c^2}{16\eta(1+k_1\phi)}\left\{1-\left(\frac{2r}{d_c}\right)^2\right\} \qquad (8)$$

where Δp is the applied pressure drop over the part L that is filled with slurry, d_c the capillary diameter, ϕ the particle volume fraction in the slurry and r the distance to the capillary axis. k_1 equals 2.5 for dilute particle suspensions, i.e. in the so-called Einstein region. At higher particle fractions, i.e. $\phi\sim\geq01$ the term $(1+k_1\phi)$ turns into $(1+k_1\phi+k^2\phi^2+\ldots)$. As soon as a sediment is formed, most of the applied

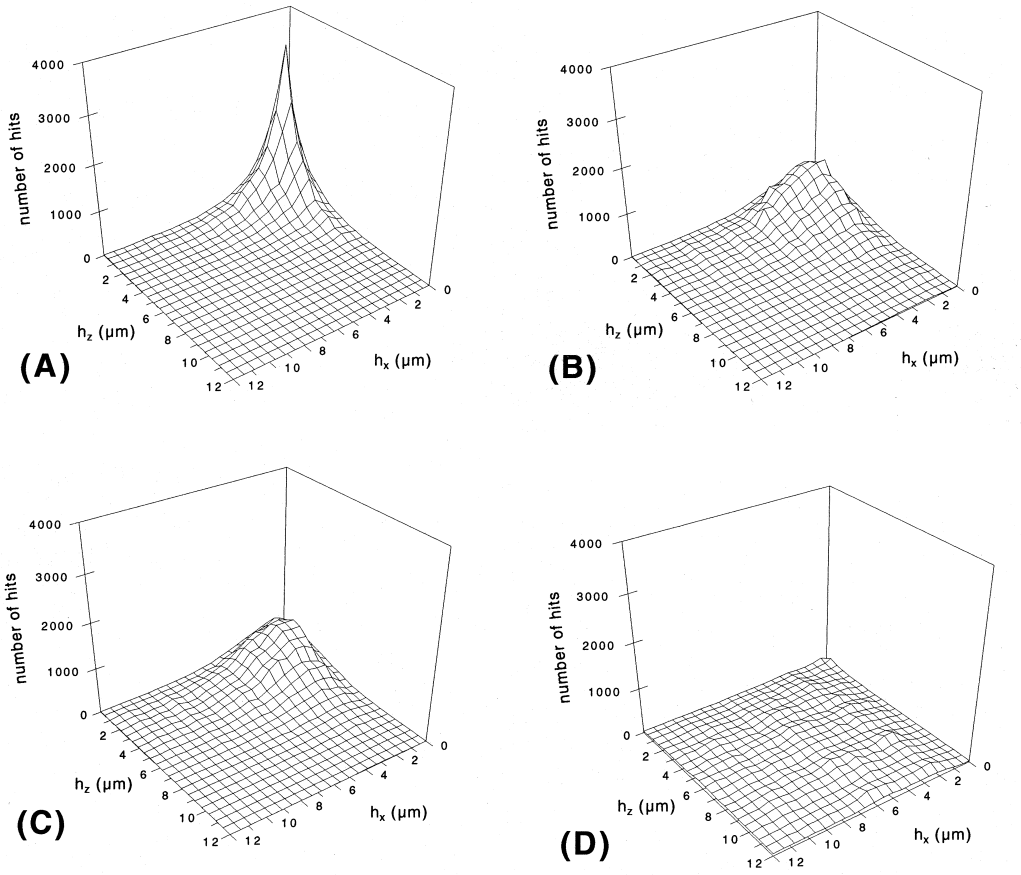

Fig. 5. Void size characterization of the bed structures obtained after simulation with a fluid velocity of $0.3 \cdot 10^{-3}$ m s^{-1} (A), $5 \cdot 10^{-3}$ m s^{-1} (B) and $11.5 \cdot 10^{-3}$ m s^{-1} (C). Graph (D) represents the characterization of the void sizes in case of a purely ballistic situation, i.e. settlement of the particles in a straight line. h_x and h_z represent the lengths of the lines that can be placed in the simulated bed structures in terms of the particle radius a in the x and z direction respectively.

pressure drop will be over the sediment. The flow field in the slurry will remain parabolic but the level of $v_z(r)$ will be reduced; it will be mainly determined by the flow resistance in the sediment, which can be described by the Carman–Kozeny equation:

$$v_0 \cong \frac{\Delta p}{h_b} \frac{a^2}{45\eta} \frac{\varepsilon_u^3}{(1-\varepsilon_u)^2} \tag{9}$$

where v_0 is the superficial velocity and h_b the height of the growing bed. Thus, the maximum velocity is proportional to h_b^{-1}. Assuming that the presence of the sediment does not change the velocity profile within the slurry near the bed, the velocity profile of the slurry v_z^s as a function of h_b and r during the column filling is given by:

$$v_z^s(r, h_s) = \frac{\Delta p}{h_b} \frac{a^2}{45\eta} \frac{\varepsilon_u^3}{(1-\varepsilon_u)^2} \left\{1 - \left(\frac{2r}{d_c}\right)^2\right\} \tag{10}$$

Obviously this is only a crude approximation of v_z^s, since Eq. (9) is not valid very close to the formed particle bed. However, it will provide information to the interpretation of the simulation experiments with respect to the filtration pressure and speed. Because of the parabolic profile within the slurry, the rate of particle deposition will be a function of r too, i.e. the deposition plane is not flat. Hence, the centre of the

column will be filled first and thereafter the regions near the wall.

Rearrangement of Eq. (10) gives a relationship that describes the deposition plane as a function of the filtration pressure Δp, radius r and the local particle deposition velocity v_d:

$$h_b = c \cdot \frac{\Delta p}{v_d} \left\{ 1 - \left(\frac{2r}{d_c} \right)^2 \right\} \quad (11)$$

where c is equal to $(a^2 \cdot \varepsilon_u^3)/(45\eta \cdot (1-\varepsilon_u)^2)$ and assumed to be constant. Application of Eq. (11) results in the figures that are depicted in Fig. 6, where the impact velocity profile is given as a function of v_d at differently applied pressure drops. The particle deposition velocity v_d was varied from $0.3 \cdot 10^{-3}$ to $80 \cdot 10^{-3}$ to m s^{-1} and Δp from 100 to 500 bar.

Inspection of the results depicted in Fig. 6 learns that in the immediate proximity of the capillary wall the particle deposition velocity v_d is always $0.3 \cdot 10^{-3}$ m s^{-1} or less. The simulation experiments show that at this particle velocity the most dense packed bed will be obtained. Note that is a purely theoretical situation. In practice, the part of the bed near the wall be distorted leading to less dense structures.

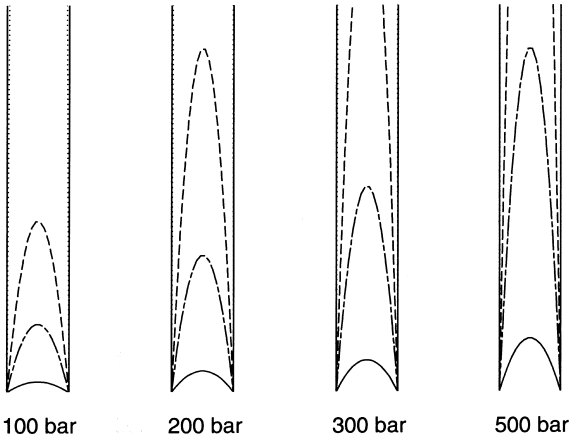

Fig. 6. Planes of constant impact velocity during the growth of the bed as a function of constant filtration pressure. Hydrodynamic regime: $v = 80 \cdot 10^{-3}$ m s^{-1} (———). Colloidal regime: $v = 11.5 \cdot 10^{-3}$ m s^{-1}, (-·-·-·-), $5 \cdot 10^{-3}$ m s^{-1} (-----) and $0.3 \cdot 10^{-3}$ m s^{-1} (·····), respectively. System parameters to calculate c were: $a = 2.65$ μm, $\eta = 0.32 \cdot 10^{-3}$ Pa s and $\varepsilon_u = 0.4$. The length of the capillary equals 40 cm.

The $0.3 \cdot 10^{-3}$ to $5 \cdot 10^{-3}$ m s^{-1} particle deposition velocity range can be seen as a transition range between a dense colloidal initial packing and the more loose hydrodynamic initial packing. Especially with lower filling pressures–i.e.< 200 bar–a considerable part of the capillaries are filled under this condition. Under such a condition a somewhat less dense bed can be expected. With higher pressures –i.e. ≥200 bar–the prevailing hydrodynamic deposition range will lead to a globally more loosely packed bed. This leads to the conclusion that most of the core of the bed has an external porosity varying with pressure, i.e. ε_u (100 bar)$<\varepsilon_u$(200 bar)$<\varepsilon_u$(300 bar)$\approx\varepsilon_u$(500 bar). Based on these results it can be concluded that increasing the filtration pressure from 100 to 500 bar will result in reducing the influence of colloidal repulsion forces. The region with the most loose bed structure is located close to the frit and near the axis of the column.

4.4. Porosity measurements and chromatographic experiments

Since the particle deposition velocity decreases during the packing of the column at constant pressure, a bed height dependent porosity is to be expected. Chromatographic techniques allow to study the total inter and intraparticle bed porosity, but do not provide information about the local porosity. Packed capillary fused-silica columns can be cut in pieces so that the porosity of the individual column pieces can be estimated. However, cutting a column will easily disturb the bed, thus affecting the porosity and was therefore not considered. Magnetic resonance imaging (MRI) is a non-destructive and non-invasive technique which can be used to measure fluid flow inside an object–either by direct measurement of the displacement of a proton-containing fluid in a well know time interval–or by mapping the effect of a contrast agent or labeled molecules [35]. Both techniques have been applied successfully to study transport phenomena in conventional and preparative high-performance liquid chromatography columns [36–40].

With MRI, proton displacements over a given time interval can be assessed. In this study the displacement of protons in the axial direction of the capillary

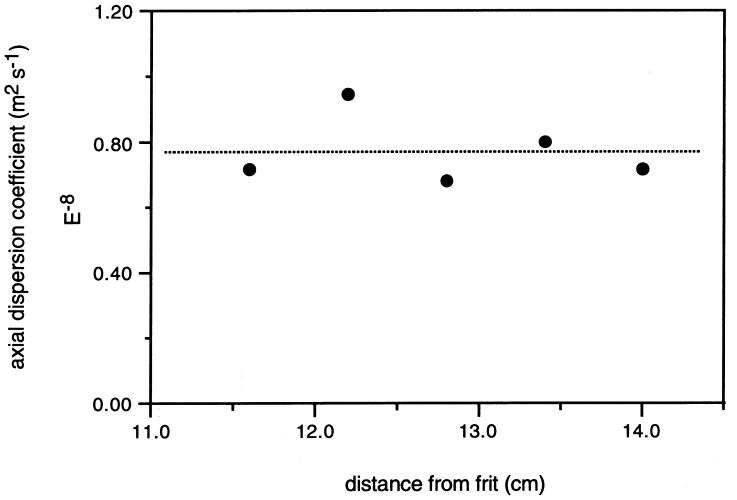

Fig. 7. Axial dispersion coefficient for different axial position, i.e. distance to the outlet frit of the column. The data represent values averaged for all radial positions probed. See the text for details.

LC columns was investigated. In case of a flow through a packed bed, such a displacement is a superposition of convective and diffusive contributions which result in a Gaussian distribution [35]. This type of MRI experiment was selected since only a few displacement profiles across the column diameter can be probed and large voids–at least for the poor chromatographic column–were to be expected.

No differences in packed-bed structures could be traced from the MRI measurements–even for columns that varied considerably in chromatographic performance, i.e. reduced plate height and column resistance factor. As an example, the axial dispersion coefficient for one of the capillaries is given as a function of the axial position in Fig. 7. The data represent values averaged for all radial positions probed.

The Gaussian-like distributed axial dispersion coefficients were found to be only slightly increased by the flow. This indicates that diffusive exchange between areas of high and low liquid velocities is fast enough to suppress any bandbroadening due to spatial variations in liquid flow through a bed. No systematic variations were found between different

Table 2
Column performance of 320-μm-I.D. capillary LC columns packed at different filtration pressures[a]; $n=2$

Filtration pressure (bar)	Compaction pressure (bar)	h	Φ	E	$K_0(10^{14}\ m^2)$	ε_t	ε_u
70	400	2.5	550	3500	5.94	0.57	0.46
100	400	2.7	510	3600	5.84	0.56	0.48
150	400	2.7	520	3700	6.06	0.56	0.48
200	400	2.4	590	3500	5.94	0.55	0.47
250	400	2.7	580	4300	5.45	0.59	0.51
300	400	2.8	510	4100	6.06	0.55	0.48
300	600	2.6	600	4000	6.32	0.53	0.47
400	600	2.6	630	4300	5.68	0.53	0.46
500	600	2.7	560	3200	5.72	0.56	0.47

[a] Acetone was the slurry liquid and acetonitrile/water (70:30, v/v) was the packing liquid. The columns were tested with an eluent composition acetonitrile/water (70:30, v/v) at 3 μl min^{-1}; the test component was anthracene (retention factor $k\sim4$).

axial or radial positions within the capillary LC column. This means that (i) no significant differences in local porosities were found on the scale of the probed volume and (ii) any inhomogeneities–e.g. small holes–that may still exist on smaller scale but they level off at the scale of the probe volume. Conclusion (i) suggests that the bed structures over almost the whole length of the measured columns are comparable and not critical with respect to the chromatographic performance of the column. This would imply that in case of the very poor chromatographically performing column–which can be due to one or a few very large voids [19]–only well packed regions were probed and defective areas were missed. The fact that according to conclusion (ii) it cannot be ruled out that inhomogeneities occur on a scale smaller that the MRI probe volume is not relevant for the column performance. Any of such disturbances do vanish on the probing scale, as is reflected by the almost Gaussian nature of the axial motion of the liquid; if it vanishes on the probing scale, it will also vanish on the capillary length scale.

The results of the packing experiments are given in Table 2, where the reduced plate height h, column resistance factor Φ, separation impedance E, total porosity ε_t and external porosity ε_u, are given for different filtration and compaction pressures. Each experiment was at least duplicated. The experimental conditions are identical to those used for the simulation experiments and are summarized in the experimental section of this paper. The slurry liquid was acetone. ε_t and ε_u, were assessed using Eq. (12) and (13) respectively [41,42].

$$\varepsilon_t = \frac{4Ft_0}{\pi d_c^2 L} \tag{12}$$

and:

$$u = \frac{\Delta p a^2}{45\psi^2 \eta L} \cdot \frac{\varepsilon_u^3}{(1-\varepsilon_u)^2} \tag{13}$$

where F is the volumetric flow, t_0 the void time of the column and ψ^2 is the particle shape factor–which is equal to 1 for spherical particles and equal to 1.7 for irregularly shaped particles.

The results given in Table 2 suggest that the filtration velocity has no influence on both the chromatographic performance and the bed porosity. The pressure during the column packing experiments was maintained on the column for 30 min. It is not unlikely that the initial bed structures of the prepared columns are in fact different, but that they vanished during the compaction process. In that case, the bed structure would be a function of the compaction pressure, which was more or less the same for all experiments. It is known from the science of soil mechanics that packed beds can be compacted by the application of a compaction pressure from the particles that transmit a 'network force' to contacting, adjacent particles. This may in fact be a large effect. When a particle from the slurry starts to become a part of the bed–i.e. at the slurry bed interface–no effective stress (except from the particle drag force) is applied to that particle. Afterwards, the whole, or a substantial part of the packing pressure acts as an effective compaction pressure on the bed. In addition, their is also a change in solvent going from the filtration to the compaction stage. Hence, the electrostatic interaction between the particles will change accordingly. Normally, however, the bed is already formed before the packing liquid reaches the particle bed. Particles that are already in the primary minimum of the DLVO curve will hardly or not at all be affected by this change in solvent [20]. Only the particles that have some degree of freedom within the 'particle network' will have the opportunity to change position.

The presence of compaction is supported by the fact that the external porosities ε_u, appear to be smaller that can be expected as based on the simulation experiments. The filtration speeds in the experiments were approximately $\geq 1 \cdot 10^{-3}$ m s^{-1}. Studying the compaction process is not an easy task, also because of the small diameter of the capillary column. A large part of the imposed compaction pressure may be resisted by friction with the capillary wall, e.g. leading to the formation of a bridge of stacked particles [43]. Thus the friction coefficient of any specific capillary-particle combination is critical.

5. Conclusions

The influence of the particle impact velocity on the chromatographic performance in slurry packing

processes can be predicted by means of a Stokesian dynamics based simulation method. The simulations indicate that a lower fluid velocity leads to a denser bed structure. This is because the velocity of freely suspended particles that are subjected to colloidal forces in the proximity of the stationary bed is mainly determined by the influence of the repulsion effects, i.e. slowing down the settling process. The external porosities of the simulated structures are below that of the densest structure if random packing exists. Hence, further compaction of the bed is still possible. The void sizes in the simulated structures are fairly small and similar in the horizontal and vertical direction. Furthermore, the radial distribution of axial velocity in the column during filling indicates that significant radial differences in bed structure are to be expected. These velocity variations also indicate that the density of the bed is expected to be higher at the frit-side of the capillary LC column.

The chromatographic experiments showed no relationships between the applied filtration pressure, the bed porosity and the performance of the capillary LC columns. The simulation experiments indicate bed structures that are dependent of the settling velocities. However, these differences vanish in a later stage, due to action of the compaction pressure. The results of this work suggest that the compaction process is the key step in the preparation of high-performance liquid chromatography columns. Knowledge about this is available in the science of soil mechanics but has not been applied to LC columns as yet.

6. Nomenclature

a	particle radius
d_c	column diameter
d_p	particle diameter
f	force per units mass
h	reduced plate height
h_b	bed height
h_{ij}	particle-to-particle distance
k_1	constant
m	mass
p	hydrodynamic pressure
r	distance
t	time
t_0	void time of a column
v	velocity
v_0	superficial velocity
v_d	$v_z(r)$ at surface of the bed
$v_z(r)$	fluid velocity
$v_z^s(r, h_b)$	velocity profile of the slurry
A_{12}	Hamaker constant
E	separation impedance
F_H	hydrodynamic force
F_B	Brownian force
F_P	colloidal interaction force + gravity
L	length
Re	Reynolds number
T	tensor
V	volume
ε_0	permittivity of vacuum
ε_r	relative dielectric constant
ε_t	total porosity
ε_u	inter-particle porosity
ϕ	particle fraction
η	fluid viscosity
κ^{-1}	double layer thickness
ρ	fluid density
ψ^2	particle shape factor
Δp	pressure drop
Φ	column resistance factor
Ψ	surface potential
∇	differential vector operator

Acknowledgements

The authors wish to thank Henk Van As, Adrie de Jager and Tom Scheenen of the NMR Centre of the Department of Molecular Physics, Wageningen Agricultural University for their assistance and support.

References

[1] M. Verzele, J. Chromatogr. 295 (1984) 81.
[2] F. Francolini, C. Borra, M. Novotny, Anal. Chem. 59 (1987) 2428.
[3] K.E. Karlsson, M. Novotny, Anal. Chem. 60 (1988) 1662.
[4] R.T. Kennedy, J.W. Jorgenson, Anal. Chem. 61 (1989) 1128.
[5] H. Menet, P. Gareil, M. Caude, R. Rosset, Chromatographia 18 (1984) 73.

[6] A. Capiello, P. Palma, F. Mangani, Chromatographia 32 (1991) 389.
[7] S.M. Han, D.W. Armstrong, Anal. Chem. 59 (1987) 1583.
[8] K. Masaharu, Y. Mon, T. Amano, Anal. Chem. S7 (1985) 2235.
[9] Y. Guan, L. Zhou, Z. Shang, J. High Resolut. Chromatogr. 15 (1992) 434.
[10] G. Crescentini, A.R. Mastrogiacomo, J. Microcol. Sep. 3 (1991) 539.
[11] G. Crescentini, F. Bruner, F. Mangani, Y. Guan, Anal. Chem. 60 (1988) 1659.
[12] A. Malik, W. Li, M.L. Lee, J. Microcol. Sep. 5 (1993) 361.
[13] W. Li, A. Malik, M.L. Lee, J. Microcol. Sep. 6 (1994) 557.
[14] D. Tong, K.D. Bartle, A.A. Clifford, J. Microcol. Sep. 6 (1994) 249.
[15] D. Tong, K.D. Bartle, A.A. Clifford, A.M. Edge, J. Microcol. Sep. 7 (1995) 26S.
[16] R. Trones, A. Iveland, T. Greibrokk, J. Microcol. Sep. 7 (1995) 505.
[17] P. Koivisto, R. Danlelsson, K.E. Markides, J. Microcol. Sep. 9 (1997) 87.
[18] D.C. Shelly, T.J. Edkins, J. Chromatogr. 411 (1987) 185.
[19] J.P.C. Vissers, H.A. Claessens, J. Laven, C.A. Cramers, Anal. Chem. 67 (1995) 2103.
[20] J.P.C. Vissers, J. Laven, H.A. Claessens, C.A. Cramers, W. Agterof, Colloids Surf A: Physicochem. Eng. Aspects. 126 (1997) 33.
[21] J.C. Gluckman, A. Hirose, V.L. McGuffin, M. Novotny, Chromatographia 17 (1983) 303.
[22] R.F. Meyer, R.A. Hartwick, Anal. Chem. 56 (1984) 2211.
[23] D.C. Shelly, V.L. Antonucci, T.J. Edkins, T.J. Dalton, J. Chromatogr. 458 (1989) 267.
[24] S.A. Karapetyan, L.M. Yakashina, G.G. Vasijarov, V.V. Braznikov, J. HRC&CC 8 (1985) 148.
[25] H. Guan-Sajonz, G. Guiochon, J. Chromatogr. A 743 (1996) 247.
[26] T. Zimina, R.M. Smith, P. Meyers, B.W. King, Chromatographia 40 (1995) 662.
[27] T. Zimina, R.M. Smith, J.C. Highfield, R. Meyers, B.W. King, J. Chromatogr. A 728 (1996) 33.
[28] W.B. Russel, D.A. Saville, W.R. Schowalter, in: W.B. Russel, D.A. Saville, W.R. Schowalter (Eds.), Colloidal Suspensions, Cambridge University Press, 1991, p. 117.
[29] L. Durlofsky, J.F. Brady, G. Bossis, J. Fluid. Mech. 180 (1987) 21.
[30] K. Hinsen, Computer Phys. Commun. 88 (1995) 327.
[31] B. Cichiocki, B.U. Felderhof, K. Hinsen, E. Wainryb, J. Blawzdziewicz, J. Chem. Phys. 100 (1994) 3780.
[32] H.C.W. Donker, H. Van As, H.J. Snijder, H.T. Edzes, Magn. Reson. Imaging 15 (1997) 113.
[33] D. van Dusschoten, P.A. de Jager, H. Van As, J. Magn. Reson., series A 116 (1995) 22.
[34] J.P. Foley, J.G. Dorsey, Anal. Chem. 55 (1983) 730.
[35] H. Van As, D. van Dusschoten, Geoderma 80 (1997) 389.
[36] U. Tallarek, E. Baumeister, K. Albert, G. Guiochon, J. Chromatogr. A 696 (1995) 1.
[37] E. Bayer, E. Baumeister, U. Tallarek, K. Albert, G. Guiochon, J. Chromatogr. A 704 (1995) 37.
[38] U. Tallarek, K. Albert, E. Bayer, G. Guiochon, AIChE J. 42 (1996) 3041.
[39] U. Tallarek, E. Bayer, G. Guiochon, 3, Am. Chem. Soc. 120 (1998) 1494.
[40] U. Tallarek, D. van Dusschoten, H. Van As, G. Guiochon, E. Bayer, Angew. Chem. Int. Ed. 37 (1998) 1882.
[41] P.A. Bristow, J. Knox, Chromatographia 10 (1977) 279.
[42] C.A. Cramers, J.A. Rijks, C.P.M. Schutjes, Chromatographia 14 (1981) 439.
[43] K. Rietema, The Dynamics of Fine Powders, Elsevier Applied Science, 1991.